THE SHADOW OF THE BH IN M87

EHT Results

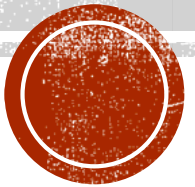

M87 – EHT ON APJL

First M87 Event Horizon Telescope Results. I. The Shadow of the Supermassive Black Hole

The Event Horizon Telescope Collaboration *et al.* 2019 *ApJL* **875** L1

Overview and Main results

First M87 Event Horizon Telescope Results. II. Array and Instrumentation

The Event Horizon Telescope Collaboration *et al.* 2019 *ApJL* **875** L2

First M87 Event Horizon Telescope Results. III. Data Processing and Calibration

The Event Horizon Telescope Collaboration *et al.* 2019 *ApJL* **875** L3

First M87 Event Horizon Telescope Results. IV. Imaging the Central Supermassive Black Hole

The Event Horizon Telescope Collaboration *et al.* 2019 *ApJL* **875** L4

Mostly technical

First M87 Event Horizon Telescope Results. V. Physical Origin of the Asymmetric Ring

The Event Horizon Telescope Collaboration *et al.* 2019 *ApJL* **875** L5

First M87 Event Horizon Telescope Results. VI. The Shadow and Mass of the Central Black Hole

The Event Horizon Telescope Collaboration *et al.* 2019 *ApJL* **875** L6

Models and interpretation

ApJ Letters

M87 AS OBSERVED BY EHT

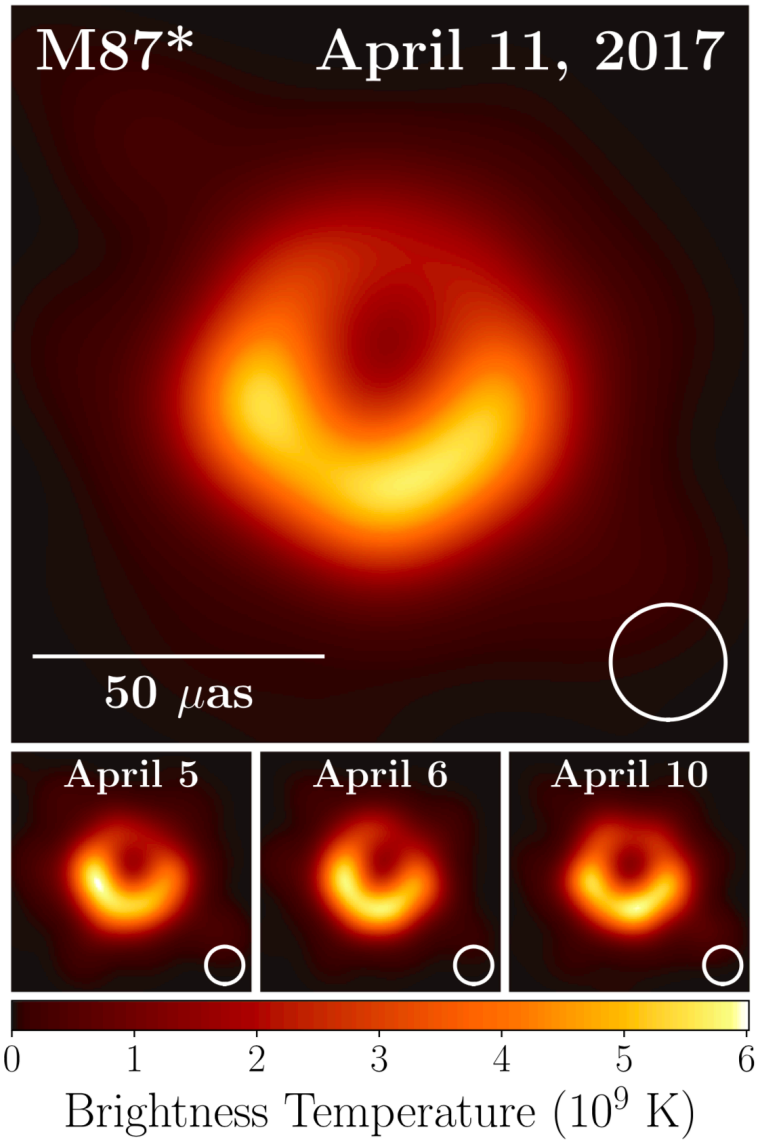

EHT observational campaign: 5-10 April, 2017
Average of three different imaging methods

Largest Gaussian kernel adopted to convolve the images (20 μas FWHM)

Stability of the basic image structure (diameter and width of the emission ring)
The position angle increases by ~20 deg between the first two days and the last two days

$$T_{\rm b} = S\,\lambda^2 \,/\, 2\,k_{\rm B}\,\Omega$$

EHT: EVENT HORIZON TELESCOPE

Already available facilities (single-dish + arrays)

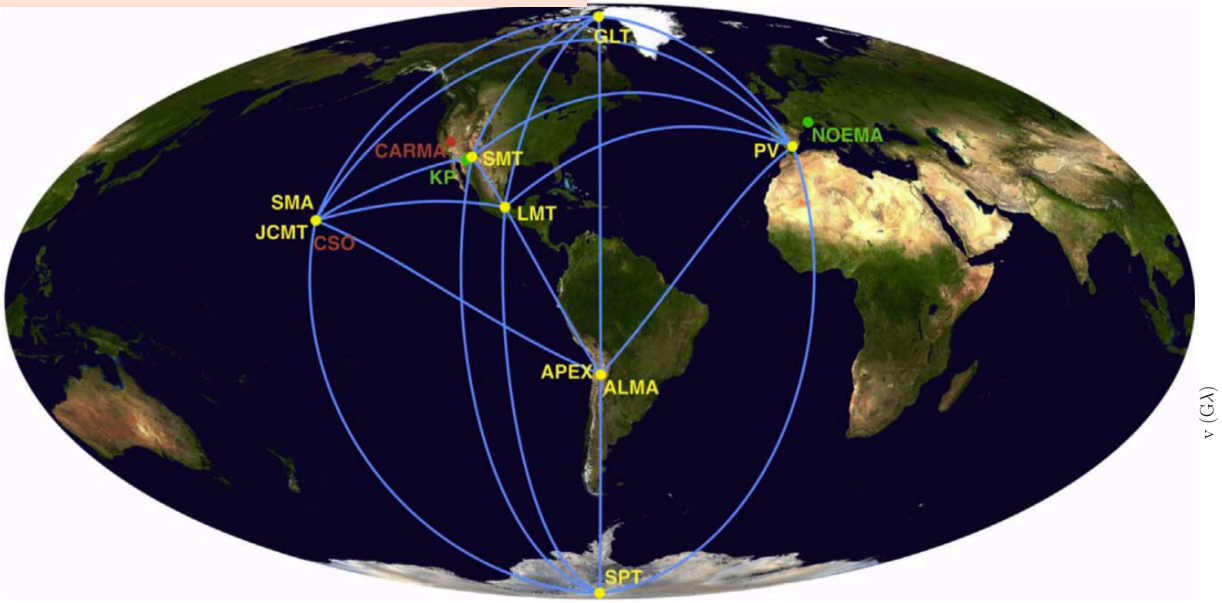

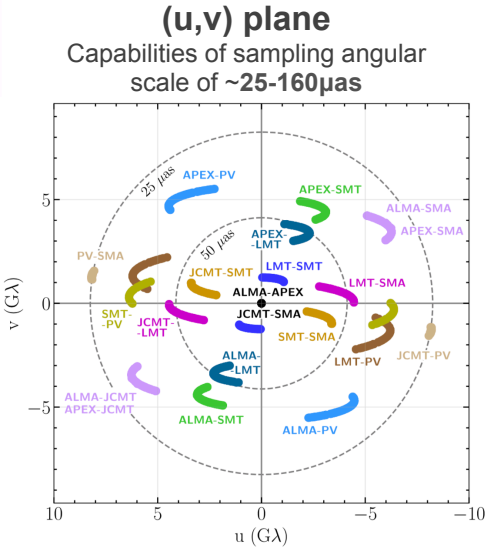

			elevation
ALMA[b]	12 (×54) and 7 (×12)	Chile	5074.1
APEX	12	Chile	5104.5
JCMT	15	Hawaii, USA	4120.1
LMT	50	Mexico	4593.3
PV 30 m	30	Spain	2919.5
SMA[b]	6 (×8)	Hawaii, USA	4115.1
SMT	10	Arizona, USA	3158.7
SPT[c]	10	Antarctica	2816.5

Facilities of the 2017 EHT campaign (**1.3mm**)

THE SITUATION AS 2019

Other high-resolution facilities

- **GRAVITY** (near-IR): relative astrometry of ~10μas, traces relativistic motion of material close to SgrA* (2018). It cannot provide spatially resolved images of the BH because of its 3 mas resolution. Recent results on NGC1068 (0.2 pc resolution, see next slides), SgrA* region, […]

- **RadioAstron** (satellite, Earth-space VLBI): ~10μas angular resolution but at longer wavelengths, not able to penetrate the self-absorbed synchrotron plasma surrounding the event horizon.

Requirements to 'observe' the BH shadow (hence, with EHT)**:**

- Sufficient number of emitted photons to illuminate the BH
- Emission coming close enough to the BH to be gravitationally lensed around it
- The surrounding plasma is sufficiently transparent at the observed frequency

+ **high spatial resolution**
SgrA* and M87: SMBHs with the largest apparent angular sizes (SgrA*: close; M87: supermassive)

For nearby low-luminosity AGN accreting via an ADAF (radiatively inefficient flow), millimeter observations are needed

NGC1068 SEEN BY GRAVITY

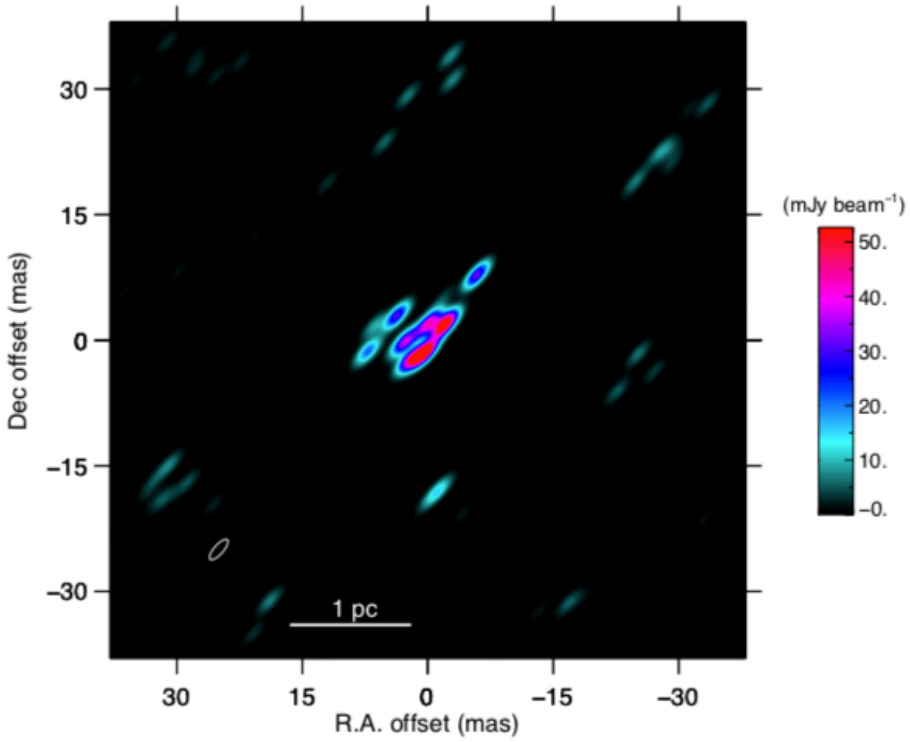

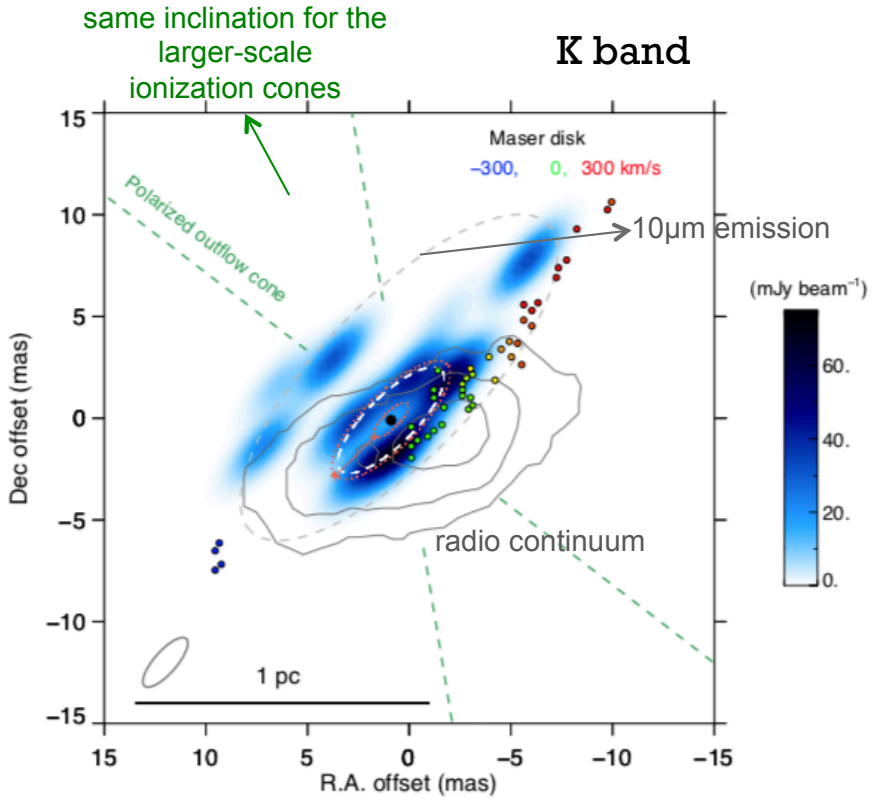

Gravity Collaboration 2020

sublimation region (R≈0.24pc)

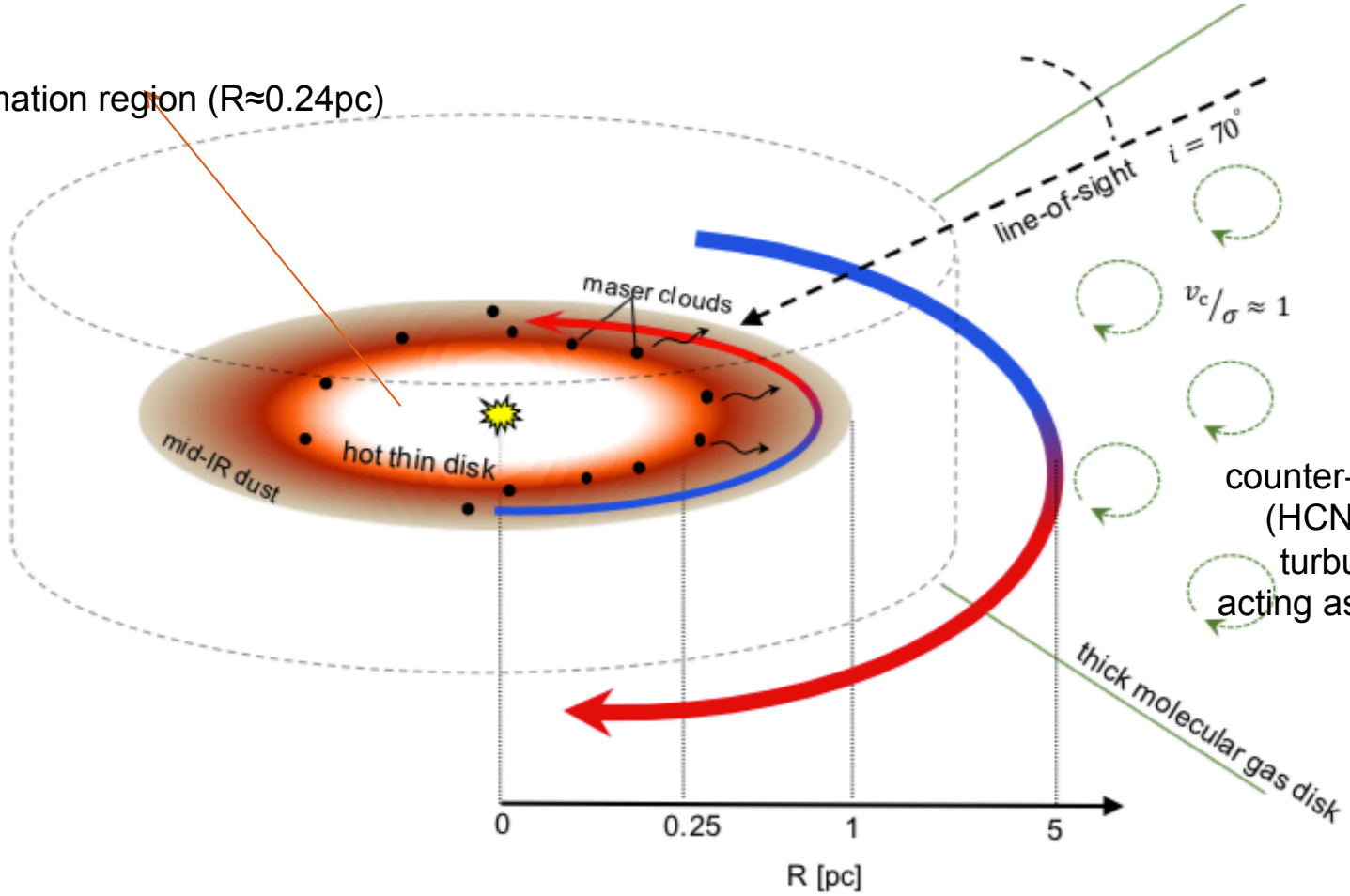

counter-rotating thick disk (HCN, HCO^+), with a turbulent structure, acting as a screen (A_V≈90)

KEY OBSERVATIONAL FACTORS

- **Angular resolution:** below 50 μas for SgrA* and M87
- **Fourier coverage:** sufficient sampling of VLBI baseline lengths and orientations to produce images with horizon-scale resolution
- **Atmospheric transparency:** high-altitude sites, submm wavelengths
- **Optically thin accretion:** SEDs of the accretion flow are due to optically thin emission (synchrotron most likely)
- **Interstellar scattering:** blurring due to insterstellar scattering by free electrons decreases with wavelengths and has limited impact in the millimeter

CHALLENGES AT SHORTER WAVELENGTHS

- Increased noice in radio receiver electronics
- Higher atmospheric opacity
- Increased phase fluctuations caused by atmospheric turbolence; the characteristic atmospheric coherence timescale is only a few seconds at mm wavelengths, and sensitivity should be able to track phase variations over correspondingly short timescales
- Decreased efficiency and size of radio telescopes in the millimeter and sub-mm

NEXT

- Higher-resolution at shorter wavelengths (e.g., 0.8mm, i.e., 345 GHz, once ‘technical’ issues and problems are propertly considered and solved)
- Next-generation of space-band interferometry

SOME CONCEPTS. I

Photon capture radius (non-rotating **Schwarschild BH**): $R_C=\sqrt{27}\ R_G$ (R_G=gravitational radius=GM/c^2):

- photons approaching the BH with an impact parameter $b<R_C$ are captured and plunge into the BH;
- photons with $b=R_C$ are captured on an unstable circular orbit and produce a **lensed photon ring** (not necessarily coincident with the ISCO);
- central flux depression is the so-called **BH shadow** corresponding to lines of sight that terminate on the event horizon.

Kerr BH (rotating BH): R_C changes with the ray's orientation relative to the angular-momentum vector, and the BH's cross section is not necessarily circular (by a few %)

maximally spinning BH (viewed face-on) – non-spinning BH

Φ (**shadow diameter**)=4.8−5.2 R_S (R_S=Schwazschild radii=$2GM/c^2$),

(~19-38 μas for M87)

over all BH spins and orientations (Bardeen1973)

SOME CONCEPTS. II

Luminet (1979): for a BH embedded in a geometrically thin, optically thick accretion disk, the photon capture radius would appear to a distant observer as a *thin emission ring* inside a lensed image of the accretion disk.

For accreting BHs embedded in a **geometrically thick, optically thin emission** region (**LLAGN** case), the combination of an **event horizon** and **light bending** leads to the appearance of a **dark shadow along with a bright emission ring**, possibly detectable with VLBI (Falcke+2000).

UNDERLYING EMISSION. I

Accretion flow as a function of the accretion rate
(Yuan & Narayan 2014; Esin et al. 1997)

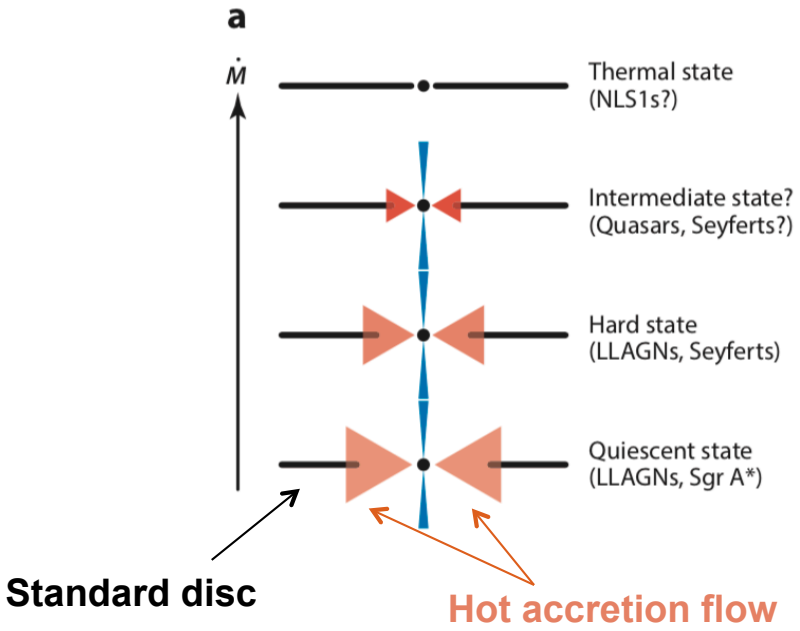

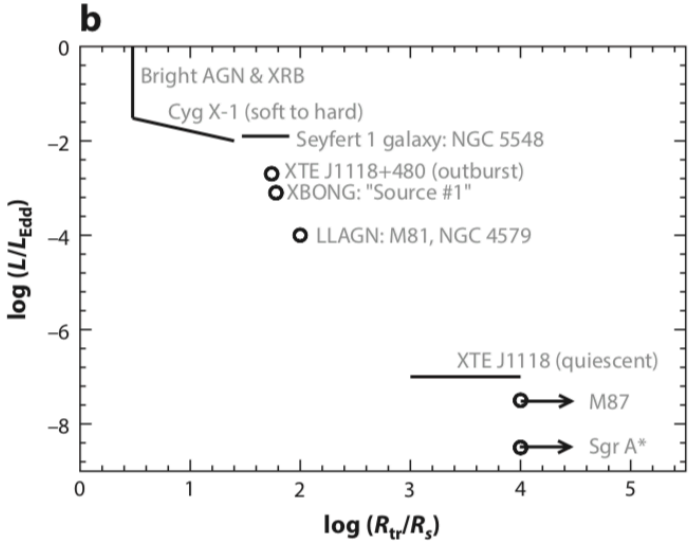

R_{tr}=transition radius
(std AD – hot flow), where the thin disc is truncated

UNDERLYING EMISSION. II

Model spectra of hot thermal accretion flows (ADAF solutions; Yuan & Narayan, ARA&A, 2014)

$\dot{m}_{\rm BH} =$

8×10^{-6},
5×10^{-5},
1.6×10^{-4},
8×10^{-4},
2.4×10^{-3}
(*bottom to top*)

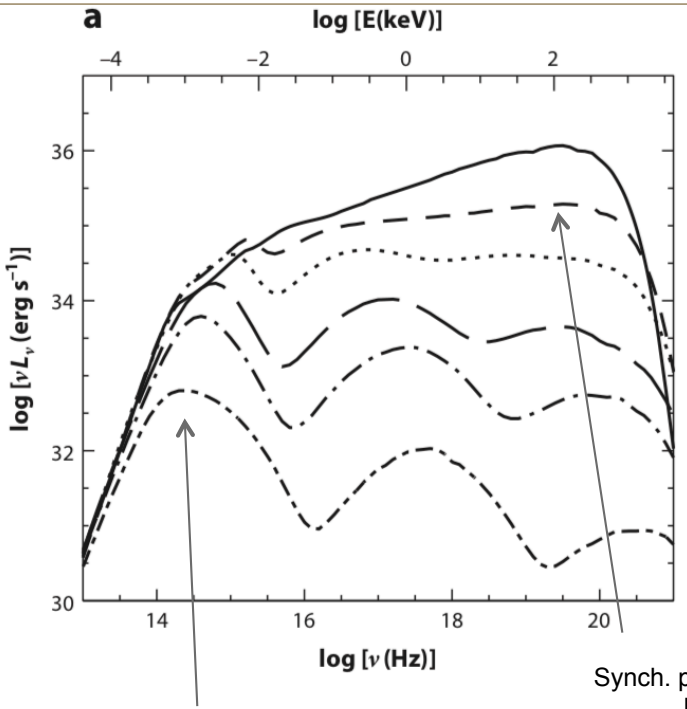

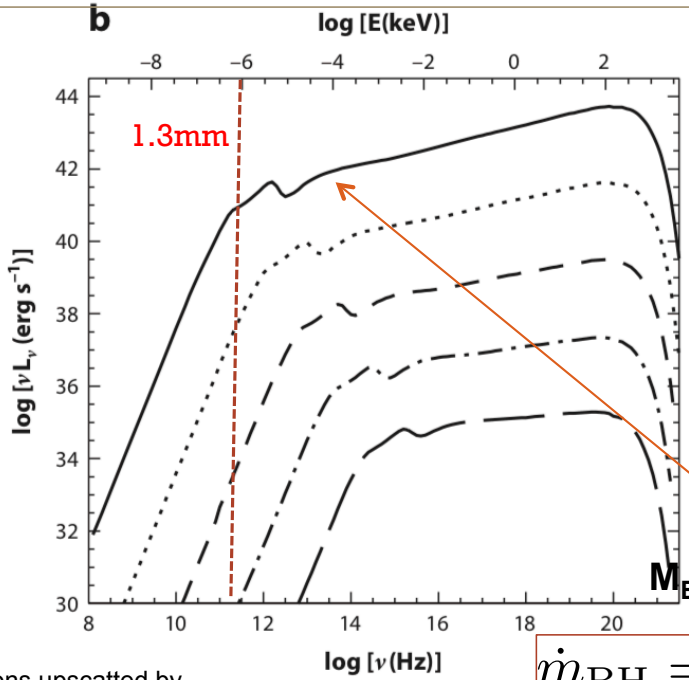

$M_{BH}/M_\odot=$

10^3,
10^5,
10^7,
10^9
(*bottom to top*)

M_{BH}(M87)~6×10^9 $M_\odot$

10-$M_\odot$ BH

Synch emission from thermal electrons
Peak from emission close to the BH

$\nu_{\rm peak} \propto \dot{m}^{1/2}\ m^{-1/2}$

Synch. photons upscatted by hot electrons
The incidence of this inverse Compton component depends on mdot

$\dot{m}_{\rm BH} = \dot{m}/\dot{m}_{\rm Edd}$

$\dot{m}_{\rm BH} = 2.4 \times 10^{-3}$

D=16.8±0.8 Mpc

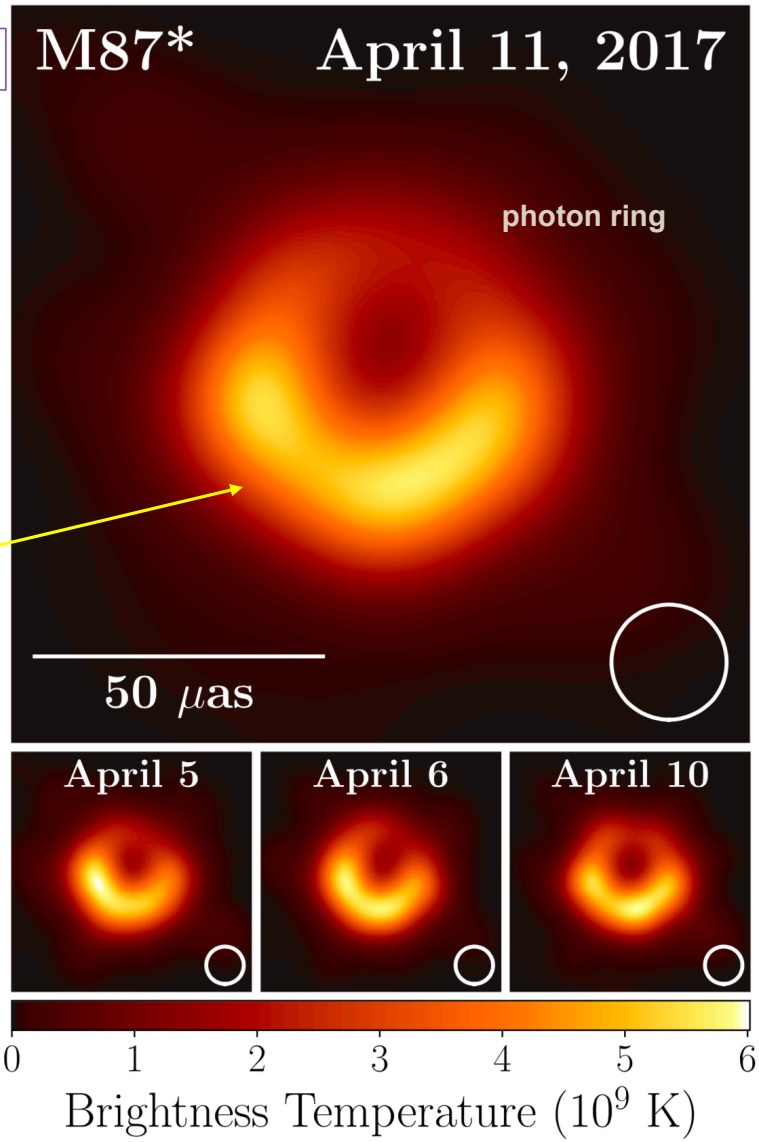

Relativistic beaming of material rotating in che clockwise direction as seen by the Earth (bottom part towards us)

S_{tot}=0.5 Jy

- Asymmetrical bright emission resolved into a **ring** (**crescent**) with **diameter** of **42±3 μas**; ≤10% deviation from circularity
- **Contrast** (bright/dark, lensed photon orbit/dim central region)=**10:1**

- Shadow of the Kerr BH as predicted by General Relativity
- Asymmetry due to **relativistic beaming** from a *plasma* rotating at v~c around and very close to the BH

The observed projected diameter of the emission ring is proportional to R_C, hence to M_{BH}, and is also a function of the observing resolution, spin vector of the BH and its inclination, size and structure of the emitting region (models/ simulations required)

SOURCE GEOMETRIES

GRMHD=
General Relativity
Magnetohydrodynamic

Several geometric source models tested

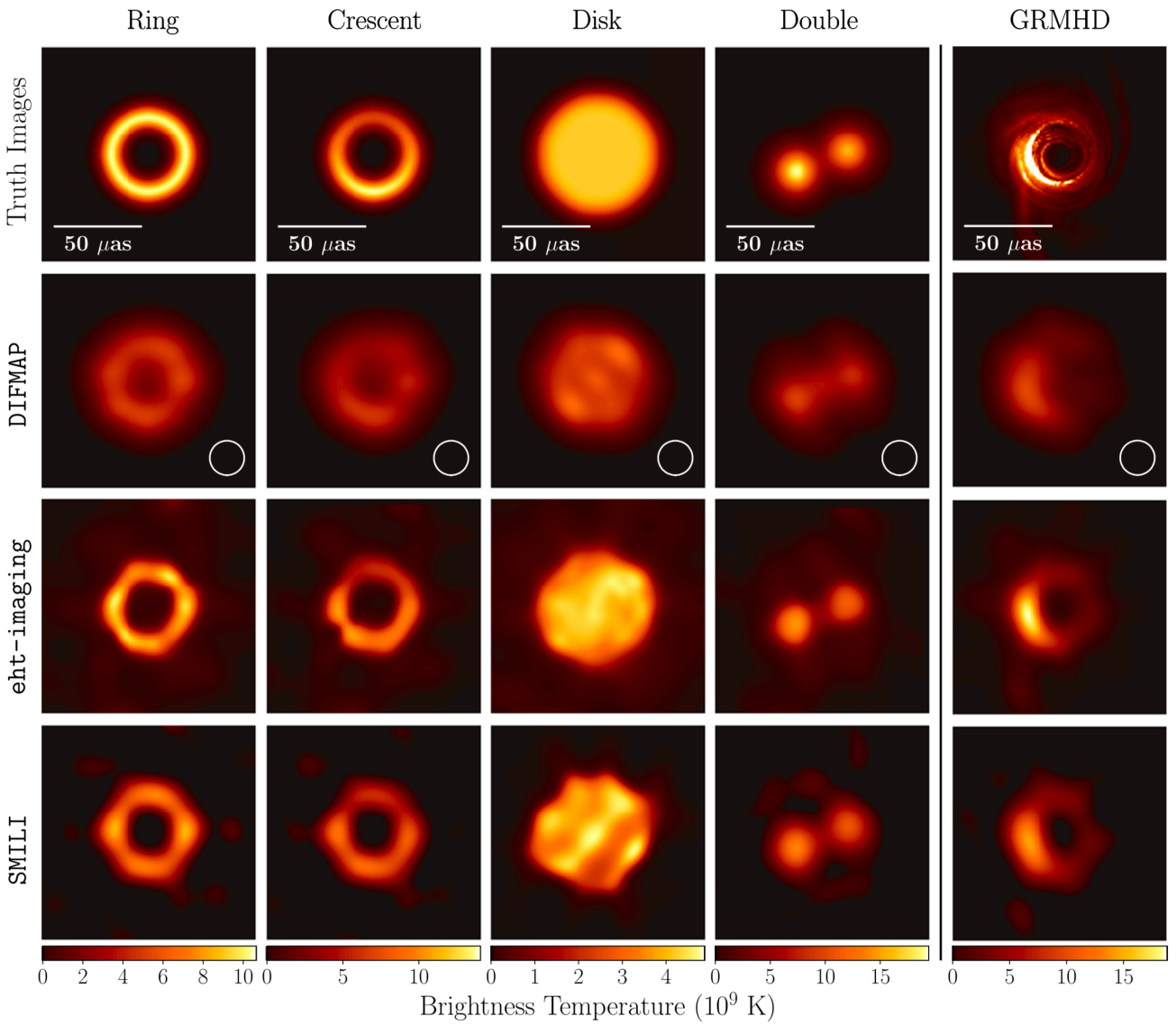

OBSERVATIONS VS. SIMULATIONS

Evolution of images on ApJ site, Paper V

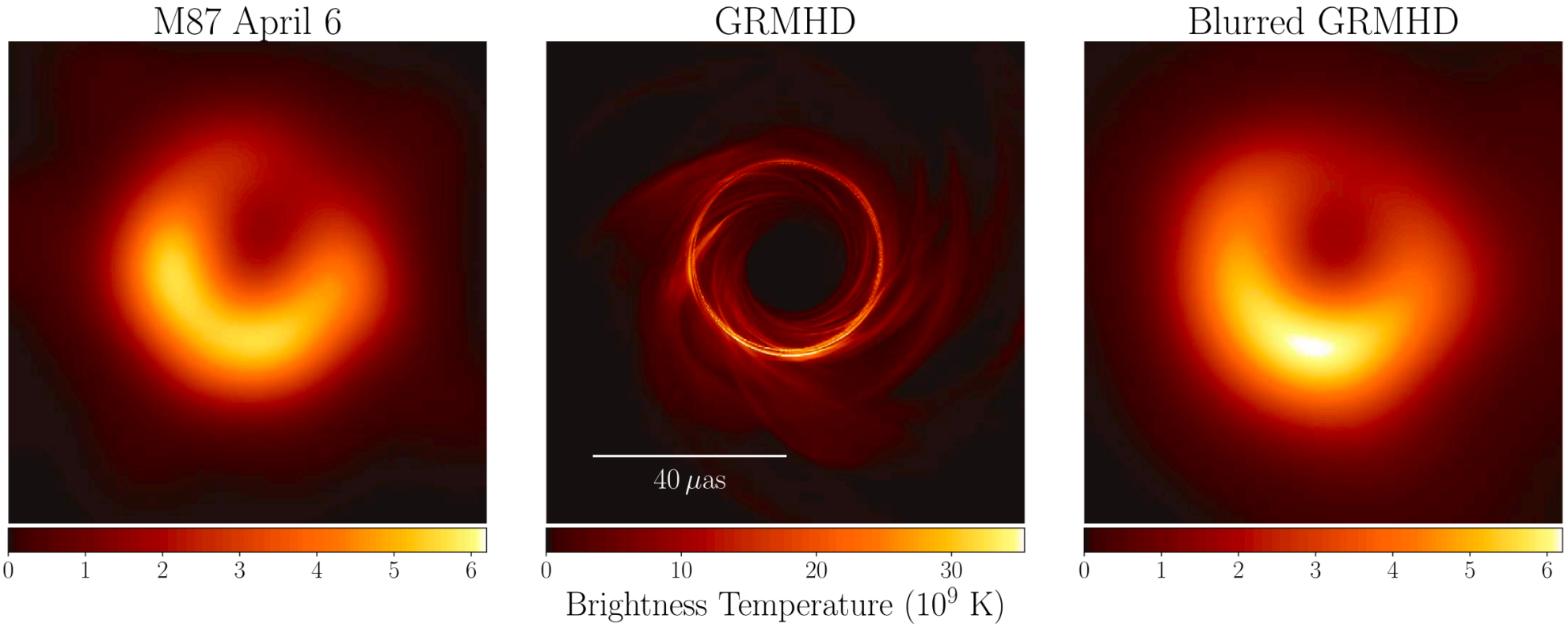

Figure 1. Left panel: an EHT2017 image of M87 from Paper IV of this series (see their Figure 15). Middle panel: a simulated image based on a GRMHD model. Right panel: the model image convolved with a 20 μas FWHM Gaussian beam. Although the most evident features of the model and data are similar, fine features in the model are not resolved by EHT.

Fine features (predicted by simulations) are not resolved by the EHT yet

i: angle between the disk angular momentum vector and the line of sight

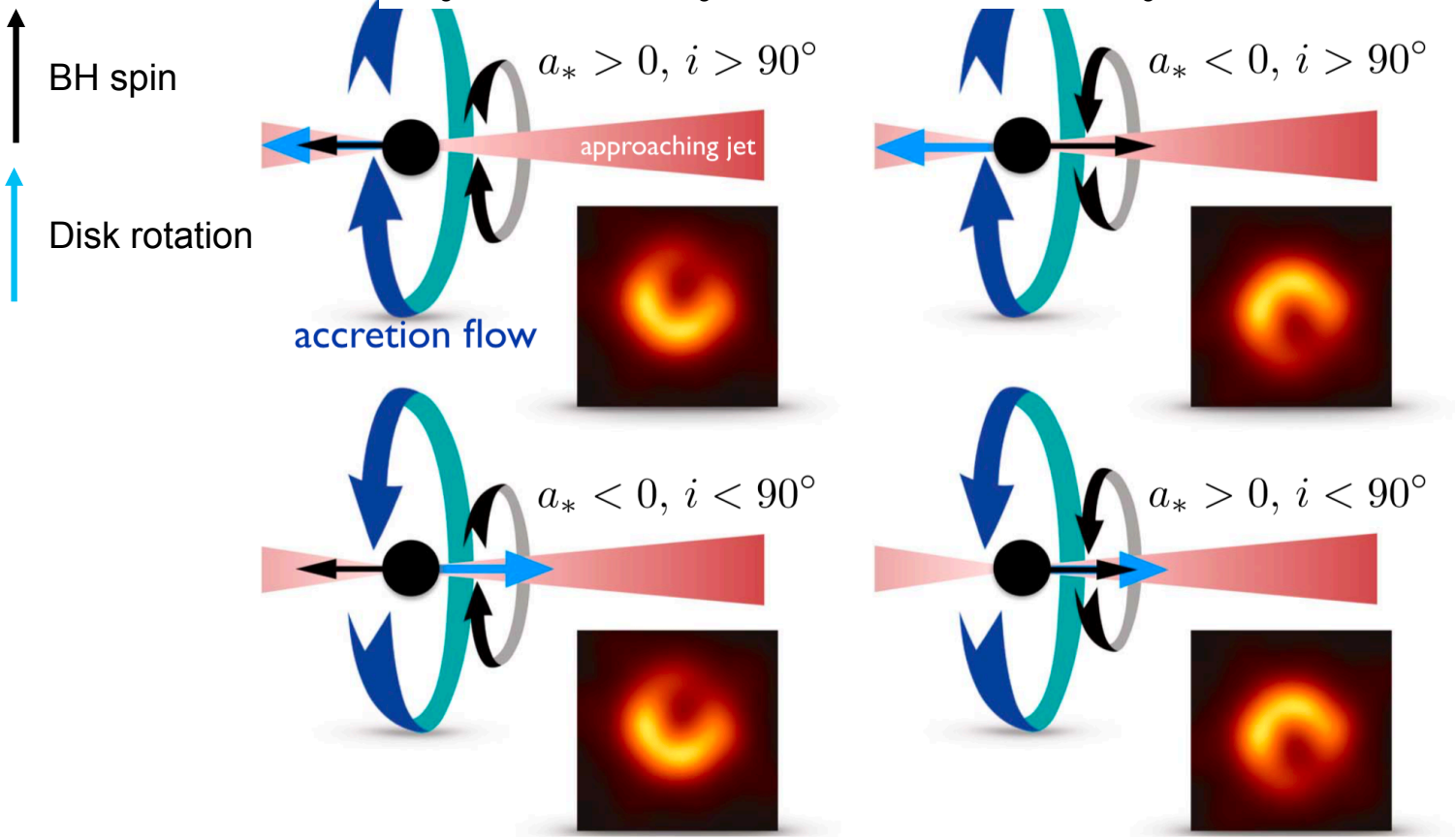

$$a_* = Jc/GM^2$$

a*: dimensionless spin
J: spin angular momentum
M: BH mass

17 deg between jet direction and line of sight

Figure 5. Illustration of the effect of black hole and disk angular momentum on ring asymmetry. The asymmetry is produced primarily by Doppler beaming: the bright region corresponds to the approaching side. In GRMHD models that fit the data comparatively well, the asymmetry arises in emission generated in the funnel wall. The sense of rotation of both the jet and funnel wall are controlled by the black hole spin. If the black hole spin axis is aligned with the large-scale jet, which points to the right, then the asymmetry implies that the black hole spin is pointing away from Earth (rotation of the black hole is clockwise as viewed from Earth). The blue ribbon arrow shows the sense of disk rotation, and the black ribbon arrow shows black hole spin. Inclination i is defined as the angle between the disk angular momentum vector and the line of sight.

THE JET IN M87

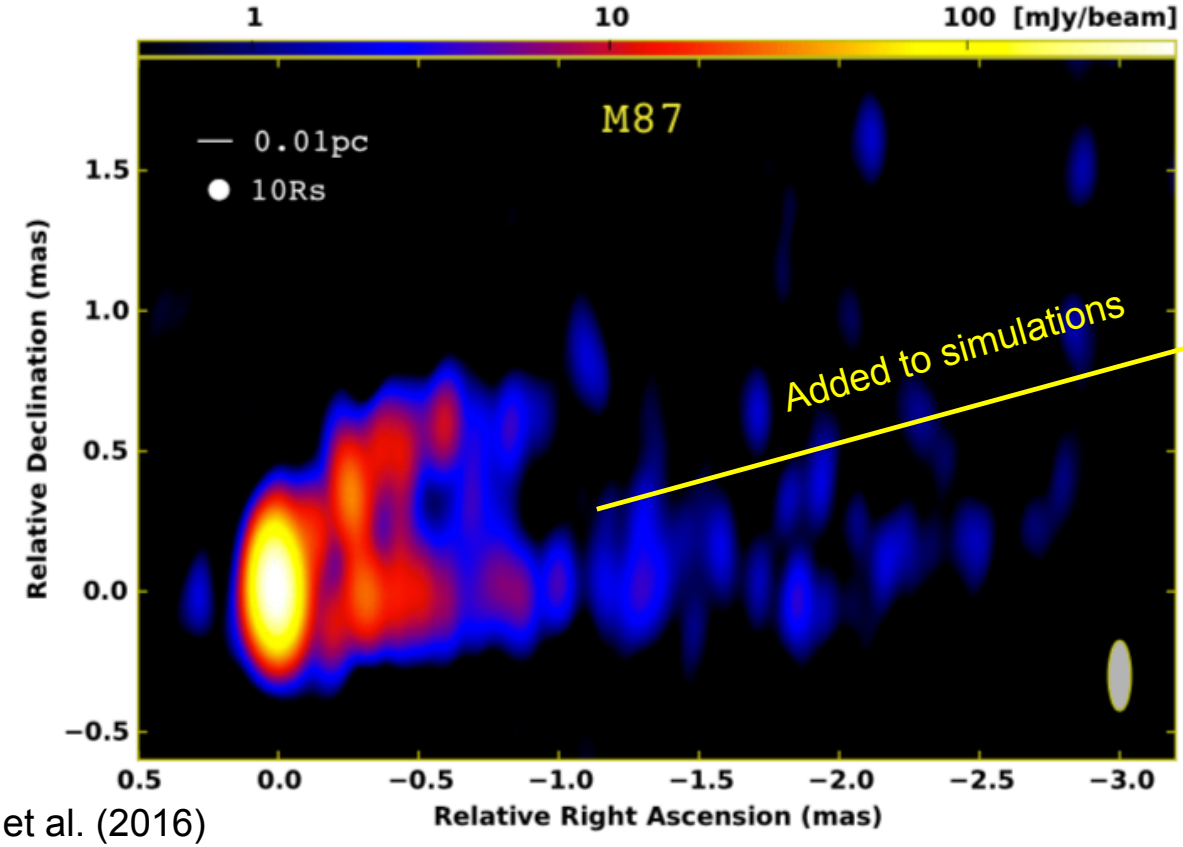

Hada et al. (2016)
VLBA+GBT, 86 GHz

Added to simulations

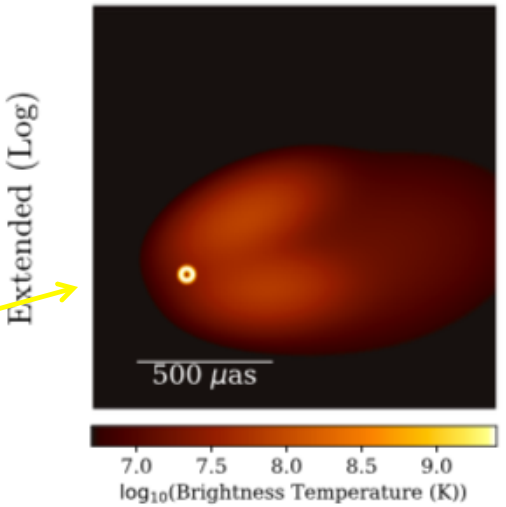

Beam=0.25×0.08 mas
Mapping ≈10 R_S scales

RESULTS

- **Constant emission** from the ring in the observational campaign, as expected
- Observed image consistent with a **magnetized accretion flow orbiting within a few R_G of the event horizon of a Kerr BH**
- North-South asymmetry in the emission ring is controlled by the BH and can be used to deduce its orientation. The BH spin is pointing away from Earth; matter in the bottom part of the image is moving towards the observer (**clockwise rotation** as seen from Earth) – consistent with the rotation of the ionized gas component observed at ~20 pc (Ford+1994; Walsh+2013)
- Non-rotating BH models are disfavored by simulation

Parameters of M87*

Parameter	Estimate
Ring diameter [a] d	42 ± 3 μas
Ring width [a]	<20 μas
Crescent contrast [b]	$>10{:}1$
Axial ratio [a]	$<4{:}3$
Orientation PA	150°–200° east of north
$\theta_g = GM/Dc^2$ [c]	3.8 ± 0.4 μas
$\alpha = d/\theta_g$ [d]	$11^{+0.5}_{-0.3}$
M [c]	$(6.5 \pm 0.7) \times 10^9\, M_\odot$

angular gravitational radius

±0.2 stat

Parameter	Prior Estimate
D [e]	(16.8 ± 0.8) Mpc
M(stars) [e]	$6.2^{+1.1}_{-0.6} \times 10^9\, M_\odot$
M(gas) [e]	$3.5^{+0.9}_{-0.3} \times 10^9\, M_\odot$

re-derived